Mechanics of Advanced Composite Structures 11 (2024) 1 – 9

Semnan University

Mechanics of Advanced Composite Structures

journal homepage: http://MACS.journals.semnan.ac.ir

Preparation, Identification, and Evaluation of the Thermal Properties of Novolac Resins Modified with TiO_2, MgO, and V_2O_5 Oxides

M. Rezaei Qazviniha, F. Piri *

Department of Chemistry, Faculty of Sciences, University of Zanjan, Zanjan, Iran.

KEYWORDS

Novolac resin;
Titanium dioxide;
Magnesium oxide;
Vanadium pentoxide;
Nanocomposite;
Thermal insulation.

ABSTRACT

It is essential to improve thermal insulation. In this study, titanium dioxide (TiO_2), magnesium oxide (MgO), and vanadium pentoxide (V_2O_5) were used as additives to modify phenolic novolac resin by the solution mixing method. Different weight percentages of resin nanoparticles (NPs) were added, and nanocomposites with different weight percentages were prepared. These nanocomposites were investigated by field emission scanning electron microscope (FE-SEM), X-ray diffraction spectroscopy (XRD), and oxyacetylene flame test (OFT). The FE-SEM images showed that the NPs were dispersed on the surface of the novolac resin at low concentrations. However, at high concentrations, the dispersion was suppressed in some cases by aggregation in the nanocomposites. The OFT test proved that by increasing the content of NPs in the nanocomposite, the back surface temperature of the sample decreased, thus improving the thermal insulation properties.

1. Introduction

Phenol formaldehyde (PF) resins, also called phenolic resins (PR), were first prepared in 1908 and are synthetic polymers obtained by reacting phenol or substituting phenol with formaldehyde [1]. PRs are a type of thermosetting resins that have attracted much attention in industrial and academic bodies due to their advantageous properties such as good stability, and high and excellent strength [2, 3]. These compounds have various applications with unique properties such as chemical and corrosion resistance, electrical insulation, high stiffness, dimensional stability, high-performance coal, low shrinkage after firing, and low production cost [4, 5].

According to the stoichiometric ratio of phenol to formaldehyde and the pH, two types of phenolic resins are distinguished, namely phenolic novolac resins and phenolic resol resins [6, 7]. When the reaction of phenol with less than equimolar proportions of formaldehyde occurs under acidic conditions, novolac resins are formed, mainly linked by methylene bridges [8]. Novolacs have good solubility, reliability, and low molecular weight [9, 10]. Crosslinking reactions increase the molecular weight of the resin, giving it valuable properties by adopting a network-like structure. However, resins generally are weak against sliding wear and thermal instability due to their low impact strength and toughness [11, 12]. Therefore, to be used in engineering applications, their structure must be modified to take advantage of the capabilities of the new polymers [7, 13].

Various techniques have been proposed to solve the above problems, including blending with elastomers, thermoplastic polymers, incorporation of nanofillers or fibers, composites, and blending of flexible chains into the polymer network [14]. The use of fillers as an additive to modify the phenolic novolac resin in the polymer matrix, which is a composite has shown remarkable achievements in this field [15, 16].

In recent years, micro-, sub-micro-, and nanoscale particles have been used as fillers to produce high-performance composites with improved properties [17-20]. Many researchers

* Corresponding author. Tel.: +98-2433052580; Fax: +98-2432282477
E-mail address: farideh.piri@znu.ac.ir

DOI: 10.22075/macs.2023.29477.1465
Received 2023-01-01; Received in revised form 2023-04-23; Accepted 2023-05-03.

have found that a wide range of metal nanoparticles (NPs) such as Ag, Au, Pd, Cu, Mn, Ni, and metal oxide NPs and ceramics such as CaO, titanium dioxide (TiO_2), magnesium oxide (MgO), vanadium pentoxide (V_2O_5), and aluminum oxide (Al_2O_3) [21-27]. These compounds can significantly improve the thermal stability, conductivity, and mechanical properties of polymer composites [28, 29]. NPs have attracted the attention of many researchers due to their diverse characteristics and thermal, mechanical, and chemical properties as well as their wide range of applications. Therefore, several studies have been carried out to use them in polymer matrices and to investigate the relationship between structure and properties in nanocomposites [30, 31]. Otta et al. investigated the MgO filler in a liquid crystalline epoxy resin matrix to develop a composite with high thermal conductivity [32]. On the other hand, Syed et al. showed that MgO microparticles have unique properties on the mechanical and thermal properties of multilayer carbon fiber-reinforced polymer composites. They found that the impact strength could be increased by about 30% in the presence of MgO fillers [33]. In another study, the mechanical properties of epoxy composites were significantly improved by adding TiO_2 particle size [34]. Moreover, the interlinear fracture toughness of flax fiber-reinforced epoxy composite was significantly improved by adding TiO_2 NPs [35]. Prasad et al. found that these fillers play an important role in improving the properties, including better thermal stability and wear resistance properties. The development of high-performance materials based on epoxy resin-based materials is encountering a growing number of requests combining high thermal stability and environmental resistance with good tribological properties. Nowadays, the use of metal oxide/novolac/fiberglass composites in the industry has solved the widespread concerns of scientists due to their high mechanical strength, excellent thermal stability, low density, good tribological performance and significant electrical resistance. Therefore, various additives such as metal oxide NP, non-porous materials, and possible molecular methods are generally used to modify the molecular structure of novolac [36].

Because of the above, the purpose of this study was to develop and apply an efficient strategy for the preparation of modified novolac resin as follows. The nanocomposites MgO/novolac/fiberglass, TiO_2/novolac/fiberglass, and V_2O_5/novolac/fiberglass were prepared with different contents of nanocomposites with 3-12 %wt in novolac resin. In this study, the improvement of the physical and thermal insulation properties of novolac resin was investigated using the solution mixing method at high temperatures.

2. Experimental

2.1. Materials

Novolac resin with a melting temperature between 105 - 115 °C and free phenol content of less than 1 (Industry and Chemical Co., Iran), 3-(trimethoxysilyl)-propylamine (Sigma Aldrich Co., United States), fiberglass type E, satin texture, with a surface density of 200 gr/m^2 (SP Systems Co., South Korea), dibutyl phthalate (DBP), TiO_2 NPs with an average particle size of 20 nm and purity greater than 99% (Degussa P25), MgO NPs with an average particle size 20 nm and purity of more than 98% (US Research Nanomaterials), and V_2O_5 NPs with an average particle size of 23 nm and purity greater than 95% (Smart Catalyst) were used as raw materials for nanocomposite fabrication. All raw materials were obtained from commercial sources and used without further processing.

2.2. Production of Nanoparticle-doped Polymer

To prepare the polymer matrix (polymer matrix for preparation of TiO_2 nanocomposites), 159 g of novolac resin was first added to 255 ml of ethanol and mixed well for one hour. Then, 15.9 g Al_2O_3 (micro), 3.75 g 3-(trimethoxysilyl)-propylamine, and 15.9 g DBP were added to the previous mixture and stirred for 5 min. The mixture is then stirred with a magnetic stirrer until a relatively thick and homogeneous brown liquid is obtained.

To prepare the polymer matrix (polymer matrix for preparing MgO and V_2O_5 nanocomposites), 318 g of novolac phenolic resin was dissolved in 510 ml of ethanol for one hour. Then 32 g Al_2O_3 (micro), 15.9 g DBP, and 7.5 g 3-(trimethoxysilyl)-propylamine were added to the solution to obtain a brown solution.

2.3. Production of Fiber-reinforced Polymer Nanocomposite

Specific amounts of TiO_2-NP (3.6, 6, and 12 wt%) are added to the resin suspension and usually. Finally, the TiO_2 NP/novolac resin mixture is unfolded on the fiberglass (the fiberglass was treated with an aqueous silane combination and dried before use) and cured at 175 °C under a pressure of 20 bar for one hour.

To prepare the nanocomposites MgO and V_2O_5, different amounts of NPs (3, 5, and 8 %wt) and (3 and 5 %wt), respectively, were added to the resin suspension mixture and mechanically mixed with a stirrer. Then, a homogeneous

mixture was prepared by the ultrasonic method. Finally, the mixture of MgO/novolac resin or V_2O_5/novolac resin NP was applied to the fiberglass (the fiberglass was treated with a blue silane mixture and dried before use) and baked at 175 °C under a pressure of 20 bar for one hour.

2.4. Characterization

The morphology of the surface of the samples was checked using a scanning electron microscope (FE-SEM) (Mira 3-XMU, Czech Republic). The composition and elements of the samples were detected by X-ray fluorescence spectroscopy using ARL™ PERFORM'X Sequential instrument. The thermal properties of the prepared samples were measured using an oxyacetylene flame test according to the ASTM E 285 standard. The crystallographic properties of the deposited NPs were recorded with X-ray diffraction spectroscopy using the BRUKER DA ADVANCE X-ray Diffractometer.

3. Results and Discussion

The TiO_2, MgO, and V_2O_5 NPs were characterized by XRD patterns to confirm the crystal structure of the phases (Figs. 1 (a)-(c)). The crystalline fraction of the NPs is 87, 93, and 59%, respectively, and they crystallize in tetragonal, cubic, and orthorhombic crystal lattices. The observed 2θ angles of 25, 38, 48, 54, 55, and 63° are the characteristics of the TiO_2 NPs synthesized in the scientific literature. The experimental XRD pattern corresponds to the number (2486-78), which indicates the anatase phase [37, 38]. The observed 2θ angles of 37, 43, 62, and 75° are characteristic of synthesized MgO NPs, and the angles of 15.5, 20.4, 26.3, and 45.5° are characteristic of fabricated V_2O_5-NPs. The XRD pattern of the produced MgO-NPs is consistent with the JCPDS card number (45-0946). No other impurities in the phases are found in the pattern [39, 40].

The XRD pattern shows a strong (002) orientation peak, indicating the high crystallinity of the produced material. Moreover, the XRD pattern of the synthesized V_2O_5 is consistent with the JCPDS card number (01-0359) [41]. It is noteworthy that no other impurity phase is found in the XRD pattern.

The XRD pattern shows a strong (110) orientation peak, indicating the average crystallinity of the synthesized material.

Moreover, the crystal size of the diffraction peaks was calculated according to the Scherer formula (1) where K (shape factor), λ (X-ray wavelength), β (full width at half maximum intensity (FWHM) in radius), θ (Bragg angle), D_{hkl} (average size) [34].

$$D = K\lambda/\beta\cos\theta \quad (1)$$

This formula was used to calculate the particle crystal sizes for the crystalline values of TiO_2, MgO, and V_2O_5 NPs, which are about 16, 44, and 23 nm, respectively.

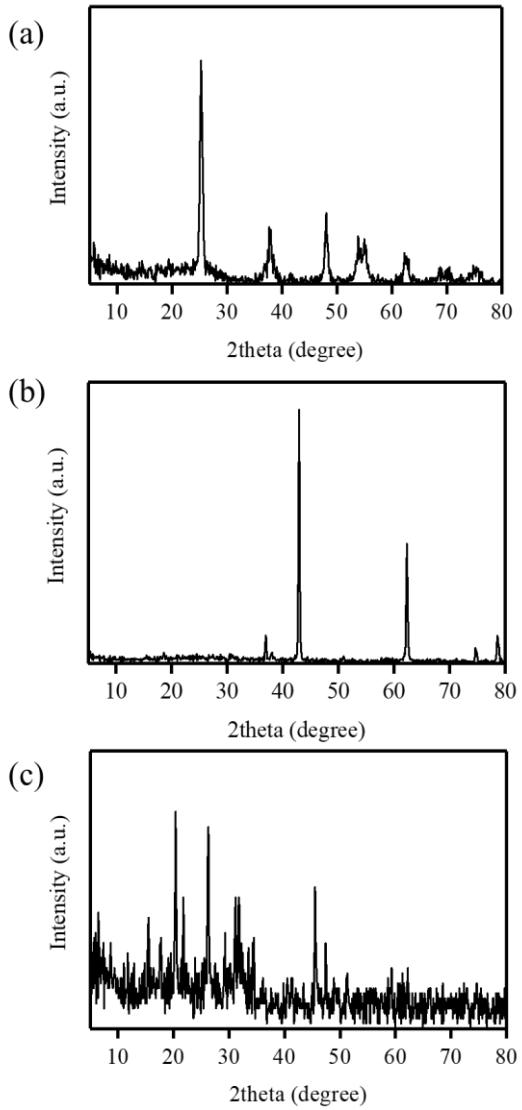

Figure 1: XRD pattern of (a) TiO_2, (b) MgO, and (c) V_2O_5 NPs.

The field emission scanning electron microscopy images (FE-SEM) of TiO_2, MgO, and V_2O_5 nanocomposites before and after the oxyacetylene flame test (OFT) are shown in Figs. 2(a)-(l). Figure 2(a) shows that the fracture surface of the novolac resin is relatively smooth and is typically a brittle material. As can be seen in the images after the flame test at 3000 °C, the structure of the novolac resin is destroyed, and the porous matrix of fiberglass plus metal oxide particles forms most of the sample (Figs. 2(b)-(c)). The SEM image micrograph (Figs. 2(d)-(f)) shows the presence of spherical and irregular peanut-like shapes, confirming the presence of TiO_2 NPs [42].

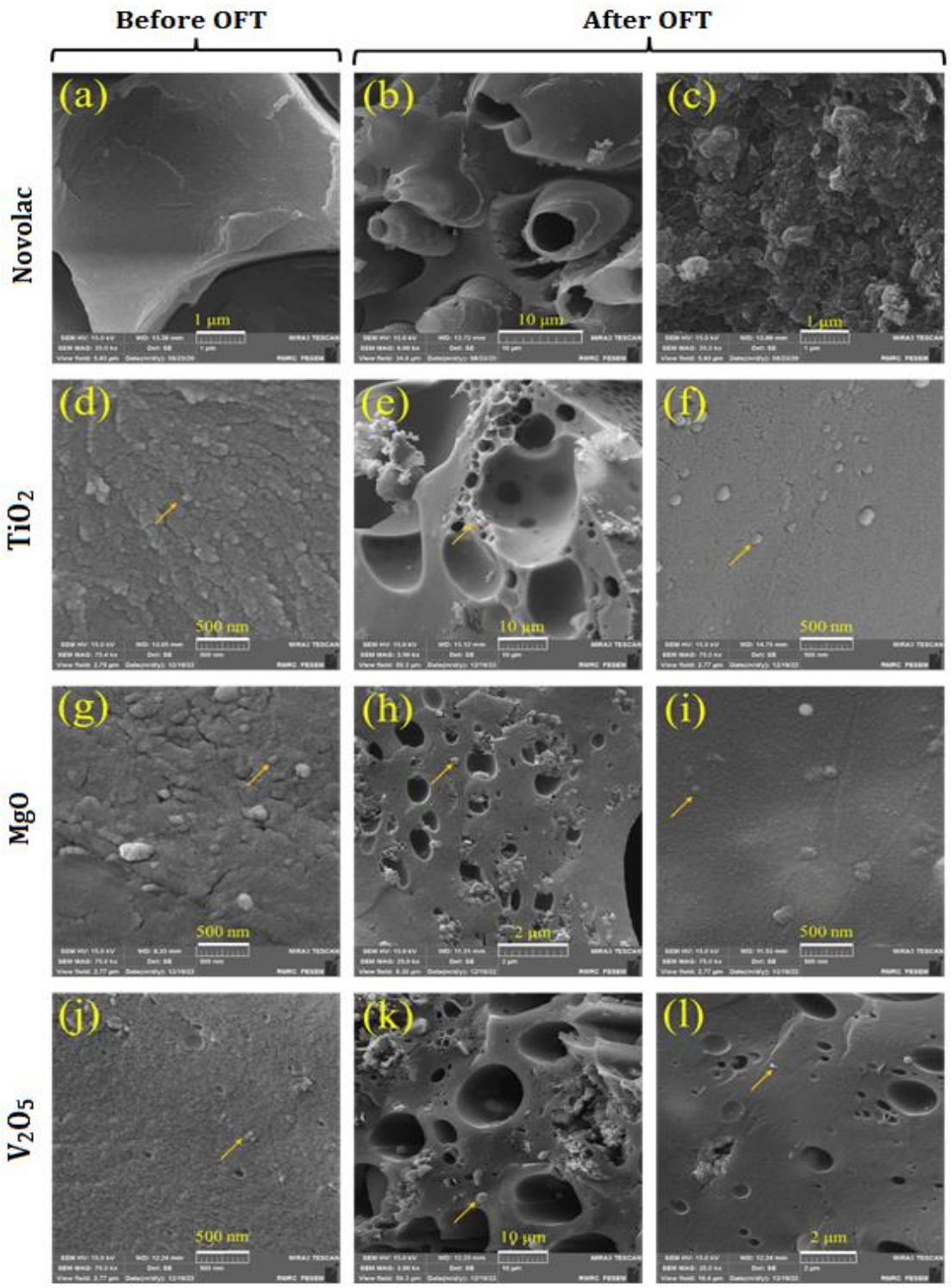

Figure 2: FE-SEM images of (a)-(c) novolac, (d)-(f) TiO_2, (g)-(i) MgO, and (j)-(l) V_2O_5 NPs before and after OFT test.

In Figs. 2(g) and (j), the nearly cubic aggregation of MgO and the spherical/rod-like morphology of V_2O_5 NPs can be easily seen [43]. For these two NPs, the average particle size is around 50 and 25 nm [44]. Moreover, in the overview, a spherical and hollow surface can be seen on the surface of the samples in the images after the flame test, indicating the formation of a carbon layer by burning the sample and the formation of a heat shield by this layer. This factor contributes significantly to the insulating property of the sample (Fig. 2(e)-(l)).

The OFT test was performed on the prepared specimens to investigate the thermal behavior and erosion performance based on the ASTM E 285 standard. The heat flux of the flame was 8500 W/m^2, and after placing the specimens at a distance of 8 mm from the tip of the flame, the temperature behind the specimens was measured over time.

The parameters affecting the thermal properties of the nanocomposite with TiO_2, MgO, and V_2O_5 NPs are listed in Table 1. As can be seen in Table 1, the specific heat capacity of these NPs is lower than that of Al_2O_3 (micro) particles. At the same time, the particle size and crystallinity fraction are positive parameters for the insulating properties of this nanocomposite. Moreover, the value of the conductivity coefficient for NPs is lower than that of Al_2O_3 (micro) particles, which also has a positive effect on insulating properties.

Thus, according to the parameters shown in Table 1, the addition of NPs, at the beginning and low temperatures did not have a significant effect on the thermal properties. However, the higher the percentage of NPs in the polymer matrix, the more positive effect it had on the thermal properties of the nanocomposite.

The results in Figs. 3(a)-(d) show that the slope of the time-temperature diagram behind the insulation and the temperature distribution on the back surface of the nanocomposites indicate that the addition of NPs (especially in the early stages of the experiment) did not have a large effect on the thermal properties. However, at times longer than 10 s, the amount of 3 %wt of NPs has a positive effect on the thermal properties of the nanocomposite. So that the thermal insulation index for the sample with 3 %wt of TiO_2, MgO, and V_2O_5 NPs is about 14, 10.5, and 7.5 s, respectively, and for the control sample, is 10, 10.5, and 8.3 s, respectively. It should be noted that this index is about 8 s for the sample with 10 %wt of TiO_2-NP.

For the sample with 3 %wt MgO-NP, the thermal insulation index at a temperature of 100 °C is almost the same as that of the control sample. However, with time and the gradual increase of temperature behind the sample, the slope of the time and temperature curve has gradually decreased. Therefore, at a temperature of 200 °C, the thermal insulation index for the sample with 3 %wt sample reaches 14 s compared to 13 s for the control sample.

Table 1. Effective parameters on thermal properties of nanocomposite containing TiO_2, MgO, and V_2O_5 NPs.

Effective particles	Al_2O_3 (Micro)	TiO_2 (Nano)	MgO (Nano)	V_2O_5 (Nano)
Specific heat capacity (J/gr. K)	0.88	0.683	0.87	0.68
Crystal size	Micro	16 nm	44 nm	23 nm
Crystallization percentage	-	87	93	59
Conductivity coefficient (W/m.K)	12.12	4.8	8	3.84

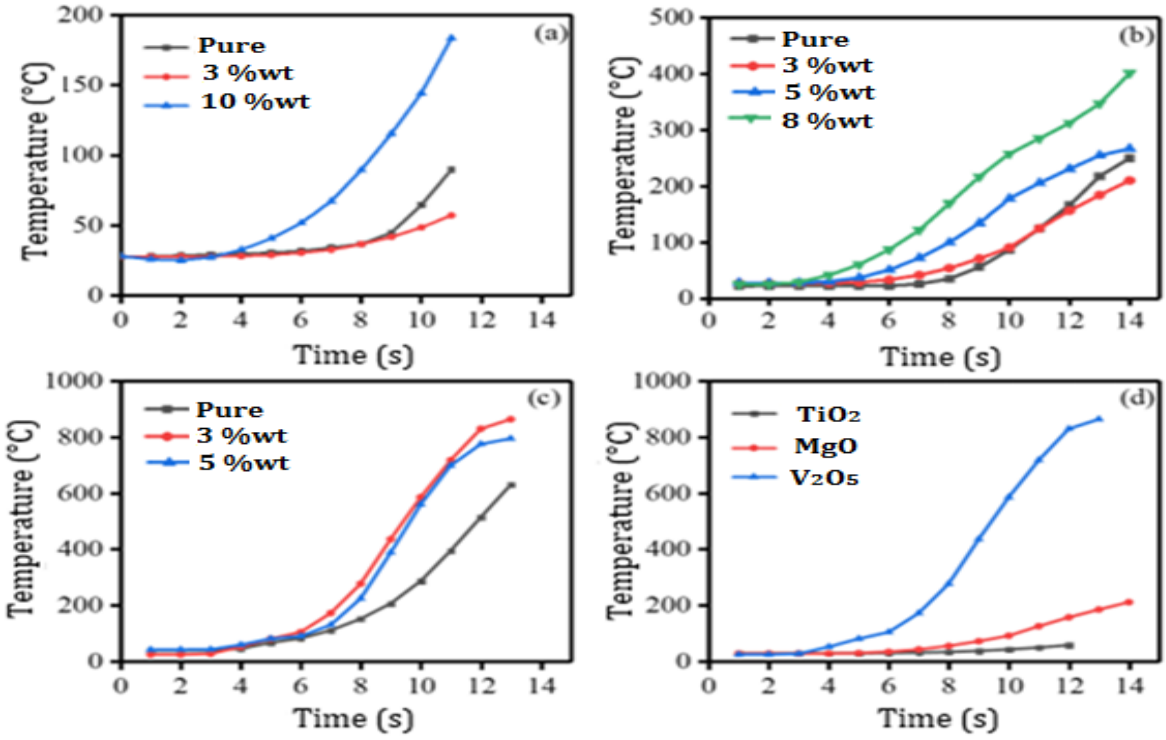

Figure 3: Temperature distribution of the back surface of (a) TiO_2, (b) MgO, (c) V_2O_5 NPs, and (d) comparison of NPs in 3 %wt, which were measured in OFT.

For the sample with 5 %wt V_2O_5, this index is about 9 s. The values presented in Table 2 clearly show the competition between the positive and negative parameters involved in the numerical value of the thermal insulation index of the nanocomposites.

Table 2. Thermal insulation index of nanocomposite containing TiO_2, MgO and V_2O_5 NPs. at 100 °C

Sample produced	Thermal insulation index (s)
Control sample (without nano)	10
TiO_2 (3 %wt)	14
TiO_2 (10 %wt)	8
Control sample (without nano)	10.5
MgO (3 %wt)	10.5
MgO (5 %wt)	8
MgO (8 %wt)	6.5
Control sample (without nano)	8.3
V_2O_5 (3 %wt)	7.5
V_2O_5 (5 %wt)	9

At low temperatures and early onset of the experiment, the positive and negative parameters do not seem to have much effect, or their effects are neutralized by each other, which led to the construction of the temperature-time diagram for all three samples.

In general, the thermal behavior at higher percentages of NPs was very similar to the sample at 3 %wt in terms of changes in the slope of the graph. However, due to the particle accumulation effect, the numerical value of the thermal insulation index parameter shows a lower value than the control sample for more significant amounts of NPs.

In the context of the OFT test method for insulation materials, one of the most critical parameters for thermal insulation is the insulation index, which corresponds to the following equation (2) where I_T (Insulation index at temperature T, (s/m)), t_T (Time for back-face temperature changes of a given temperature,(s)), d (thickness of the specimen, (m))

$$I_T = t_T/d \quad (2)$$

According to the ASTM E 285 standard, in the oxyacetylene flame test for a specimen of a given thickness, the time that elapses until the temperature behind the specimen reaches a constant value is called the insulation index. For example, the time that elapses until the temperature behind the specimen with a unit thickness reaches 100 °C is called the insulation index at 100 °C for that thickness, and its unit is s/m. It indicates how long it takes for the temperature behind the sample to reach a specific uniform size, and the better the index, the better the insulation performance.

The difference in nanocomposite performance may be due to differences in the ceramic layers formed in the OFT test. To analyze the results of this test, the surface of the samples was checked using digital images.

The digital images of the nanocomposite samples are shown in Figs. 4(a)-(h). Figure 4(a) refers to pure, and Figs. 4(b)-(h) refers to samples TiO_2 (3 %wt), TiO_2 (10 %wt), MgO (3 %wt), MgO (5 %wt), MgO (8 %wt), V_2O_5 (3 %wt), and V_2O_5 (5 %wt) NPs respectively after the OFT test. According to Fig. 4(a), the layers formed on the sample without NPs are spherical drops, which are discontinuous and pushed back by the flame. The low viscosity of these droplets has caused them to move away rapidly from the sample during the OFT flame test. This prepares the space for further destruction, ultimately increasing the erosion rate of the sample surface. As can be seen in Figs. 4(b)-(h), the presence of NPs increases the strength and continuity of the layer.

Accordingly, the viscosity of the materials formed during the experiment is so high that the flame moves less due to the strong flow, and this layer can be seen even in the parts exposed to the direct flame. Furthermore, as the amount of NPs increases, so does the amount of layer formed.

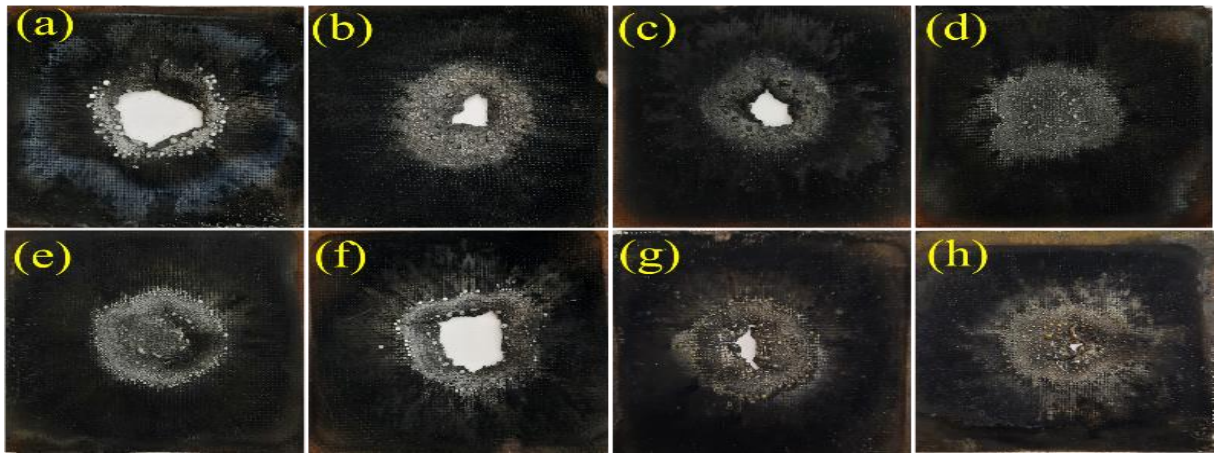

Figure 4. The digital images of (a) evident, (b) TiO_2 (3 %wt), (c) TiO_2 (10 %wt), (d) MgO (3 %wt), (e) MgO (5 %wt), (f) MgO (8 %wt), (%wt) V_2O_5 (3 %wt), and (h) V_2O_5 (5 %wt) NPs after the OFT test.

4. Conclusion

In this research, TiO_2, MgO, and V_2O_5 NPs/novolac resin/fiberglass nanocomposites were synthesized by solution mixing over different contents of nanocomposites with 3-10 wt%. The SEM, XRD, and OFT test was used to investigate the formation of nanocomposites. According to the SEM images, the average crystallite size of TiO_2, MgO, and V_2O_5 is about 16, 44, and 23 nm, respectively. The XRD patterns of TiO_2, MgO, and V_2O_5 NPs confirm tetragonal, cubic, and orthorhombic crystal structures. The difference in the performance of the nanocomposites in the OFT test showed that the presence of NPs increases the strength and cohesion of the layers. As the amount of NPs increases, the cohesion and the amount of layer formed also increase. This layer may be the reason for the improved thermal insulation properties

Acknowledgment

The authors acknowledge the University of Zanjan for financial support.

Conflicts of Interest

The author declares that there is no conflict of interest regarding the publication of this manuscript. In addition, the authors have entirely observed the ethical issues, including plagiarism, informed consent, misconduct, data fabrication and/or falsification, double publication and/or submission, and redundancy.

References

[1] Milewski, J.V. & Rosato, D.V., 1981. History of reinforced plastics. *Journal of Macromolecular Science—Chemistry, 15* (7), pp.1303-1343.

[2] Wang, M., Leitch, M. & Xu, C.C., 2009. Synthesis of phenol–formaldehyde resol resins using organosolv pine lignins. *European Polymer Journal, 45* (12), pp.3380-3388.

[3] Hussin, M.H., Abd Latif, N.H., Hamidon, T.S., Idris, N.N., Hashim, R., Appaturi, J.N., Brosse, N., Ziegler-Devin, I., Chrusiel, L. & Fatriasari, W., 2022. Latest advancements in high-performance bio-based wood adhesives: A critical review. *Journal of Materials Research and Technology*.

[4] Song, D. & Gupta, R., 2012. *The use of thermosets in the building and construction industry*. *Thermosets.* Elsevier, pp.165-188.

[5] Cheremisinoff, N.P. & Cheremisinoff, P.N., 1995. *Fiberglass reinforced plastics: Manufacturing techniques and applications*. William Andrew.

[6] Effendi, A., Gerhauser, H. & Bridgwater, A.V., 2008. Production of renewable phenolic resins by thermochemical conversion of biomass: A review. *Renewable and sustainable energy reviews, 12* (8), pp.2092-2116.

[7] Nair, C.R., 2004. Advances in addition-cure phenolic resins. *Progress in polymer science, 29* (5), pp.401-498.

[8] Kiskan, B. & Yagci, Y., 2020. The journey of phenolics from the first spark to advanced materials. *Israel Journal of Chemistry, 60* (1-2), pp.20-32.

[9] Wang, M., Yang, M., Zhao, T. & Pei, J., 2008. Acetylene-grafted resins derived from phenolics via azo coupling reaction. *European polymer journal, 44* (3), pp.842-848.

[10] Lu, Y., Ye, L., Han, W., Sun, Y., Qiu, W. & Zhao, T., 2015. Synthesis, characterization and microstructure of tantalum carbide-based ceramics by liquid polymeric precursor method. *Ceramics International, 41* (9), pp.12475-12479.

[11] Ghosh, P., Naskar, K. & Das, N.C., 2020. Influence of synthetic graphite powder on tribological and thermo-mechanical properties of organic-inorganic hybrid fiber reinforced elastomer-modified phenolic resin friction composites. *Composites Part C: Open Access, 2*, pp.100018.

[12] Dass, K., Chauhan, S. & Gaur, B., 2014. Effects of microsize sic, al2o3, and zno particulates on mechanical and tribological properties of synthesized ortho-and meta-cresol novolac epoxy composites. *Proceedings of the Institution of Mechanical Engineers, Part J: Journal of Engineering Tribology, 228* (8), pp.881-895.

[13] Rezaei Qazviniha, M. & Piri, F., 2023. Synthesis and characterization al2o3/novolac/fiberglass nanocomposite: Modification of thermal stability and thermal insulation properties. *Mechanics Of Advanced Composite Structures, 10* (1), pp.21-28.

[14] Athawale, A.A. & Pandit, J.A., 2019. Unsaturated polyester resins, blends, interpenetrating polymer networks, composites, and nanocomposites: State of the art and new challenges. *Unsaturated Polyester Resins*, pp.1-42.

[15] Ahmad, S., Ali, S., Salman, M. & Baluch, A.H., 2021. A comparative study on the effect of carbon-based and ceramic additives on the properties of fiber reinforced polymer matrix composites for high temperature applications. *Ceramics International, 47* (24), pp.33956-33971.

[16] Sandomierski, M., Strzemiecka, B., Koczorowski, W., Barczewski, M., Kasperkowiak, M., Pokora, M., Borek, B., Chehimi, M.M. & Voelkel, A., 2019. Mechanically robust and thermally stable abrasive tools from phenolic resins reinforced with diazonium-modified zeolites. *Polymer Composites, 40* (8), pp.3209-3219.

[17] Friedrich, K., 2018. Polymer composites for tribological applications. *Advanced Industrial and Engineering Polymer Research, 1* (1), pp.3-39.

[18] Chung, T.-S., Jiang, L.Y., Li, Y. & Kulprathipanja, S., 2007. Mixed matrix membranes (mmms) comprising organic polymers with dispersed inorganic fillers for gas separation. *Progress in polymer science, 32* (4), pp.483-507.

[19] Yan, S.-R., Toghraie, D., Abdulkareem, L.A., Alizadeh, A.A., Barnoon, P. & Afrand, M., 2020. The rheological behavior of mwcnts–zno/water–ethylene glycol hybrid non-newtonian nanofluid by using of an experimental investigation. *Journal of Materials Research and Technology, 9* (4), pp.8401-8406.

[20] Rostami, S., Toghraie, D., Esfahani, M.A., Hekmatifar, M. & Sina, N., 2021. Predict the thermal conductivity of sio2/water–ethylene glycol (50: 50) hybrid nanofluid using artificial neural network. *Journal of Thermal Analysis and Calorimetry, 143* (2), pp.1119-1128.

[21] Schrand, A.M., Rahman, M.F., Hussain, S.M., Schlager, J.J., Smith, D.A. & Syed, A.F., 2010. Metal-based nanoparticles and their toxicity assessment. *Wiley interdisciplinary reviews: Nanomedicine and Nanobiotechnology, 2* (5), pp.544-568.

[22] Dhand, C., Dwivedi, N., Loh, X.J., Ying, A.N.J., Verma, N.K., Beuerman, R.W., Lakshminarayanan, R. & Ramakrishna, S., 2015. Methods and strategies for the synthesis of diverse nanoparticles and their applications: A comprehensive overview. *Rsc Advances, 5* (127), pp.105003-105037.

[23] Zhan, G. & Zeng, H.C., 2016. Integrated nanocatalysts with mesoporous silica/silicate and microporous mof materials. *Coordination Chemistry Reviews, 320*, pp.181-192.

[24] Demircan, G., Kisa, M., Ozen, M. & Aktas, B., 2020. Surface-modified alumina nanoparticles-filled aramid fiber-reinforced epoxy nanocomposites: Preparation and mechanical properties. *Iranian Polymer Journal, 29* (3), pp.253-264.

[25] Ozen, M., Demircan, G., Kisa, M., Acikgoz, A., Ceyhan, G. & Işıker, Y., 2022. Thermal properties of surface-modified nano-al2o3/kevlar fiber/epoxy composites. *Materials Chemistry and Physics, 278*, pp.125689.

[26] Demircan, G., Kisa, M., Ozen, M. & Acikgoz, A., 2021. Quasi-static penetration behavior of glass-fiber-reinforced epoxy nanocomposites. *Mechanics of Composite Materials, 57* (4), pp.503-516.

[27] Boroomandpour, A., Toghraie, D. & Hashemian, M., 2020. A comprehensive experimental investigation of thermal conductivity of a ternary hybrid nanofluid containing mwcnts-titania-zinc oxide/water-ethylene glycol (80: 20) as well as binary and mono nanofluids. *Synthetic Metals, 268*, pp.116501.

[28] Saida, K., Song, W. & Nishimoto, K., 2006. Laser brazing of alloy 600 with precious filler metals. *Science and Technology of Welding and Joining, 11* (6), pp.694-700.

[29] Zhu, W., Zhang, H., Guo, C., Liu, Y. & Ran, X., 2019. Wetting and brazing characteristic of high nitrogen austenitic stainless steel and 316l austenitic stainless steel by ag–cu filler. *Vacuum, 166*, pp.97-106.

[30] Saleh, T.A., 2020. Nanomaterials: Classification, properties, and environmental toxicities. *Environmental Technology & Innovation, 20*, pp.101067.

[31] Prakash, J., Khan, S., Chauhan, S. & Biradar, A., 2020. Metal oxide-

nanoparticles and liquid crystal composites: A review of recent progress. *Journal of Molecular Liquids, 297*, pp.112052.

[32] Ota, S. & Harada, M., 2021. Filler surface adsorption of mesogenic epoxy for lc epoxy/mgo composites with high thermal conductivity. *Composites Part C: Open Access, 4*, pp.100087.

[33] Uzay, Ç., 2022. Mechanical and thermal characterization of laminar carbon/epoxy composites modified with magnesium oxide microparticles. *Polymer Composites, 43* (1), pp.299-310.

[34] Al-Turaif, H.A., 2010. Effect of nano tio2 particle size on mechanical properties of cured epoxy resin. *Progress in Organic Coatings, 69* (3), pp.241-246.

[35] Prasad, V., Sekar, K., Varghese, S. & Joseph, M., 2019. Enhancing mode i and mode ii interlaminar fracture toughness of flax fibre reinforced epoxy composites with nano tio2. *Composites Part A: Applied Science and Manufacturing, 124*, pp.105505.

[36] Kyotani, T., 2000. Control of pore structure in carbon. *Carbon, 38* (2), pp.269-286.

[37] Theivasanthi, T. & Alagar, M., 2013. Titanium dioxide (tio2) nanoparticles xrd analyses: An insight. *arXiv preprint arXiv:1307.1091*.

[38] Pratheepa, M.I. & Lawrence, M., 2017. X-ray diffraction analyses of titanium dioxide nanoparticles. *Int J Sci Res Sci Technol, 3* (11), pp.83-88.

[39] Rani, N., Chahal, S., Chauhan, A.S., Kumar, P., Shukla, R. & Singh, S., 2019. X-ray analysis of mgo nanoparticles by modified scherer's williamson-hall and size-strain method. *Materials Today: Proceedings, 12*, pp.543-548.

[40] Balakrishnan, G., Velavan, R., Batoo, K.M. & Raslan, E.H., 2020. Microstructure, optical and photocatalytic properties of mgo nanoparticles. *Results in Physics, 16*, pp.103013.

[41] Govindarajan, D., Uma Shankar, V. & Gopalakrishnan, R., 2019. Supercapacitor behavior and characterization of rgo anchored v2o5 nanorods. *Journal of Materials Science: Materials in Electronics, 30* (17), pp.16142-16155.

[42] Arami, H., Mazloumi, M., Khalifehzadeh, R. & Sadrnezhaad, S., 2007. Sonochemical preparation of tio2 nanoparticles. *Materials Letters, 61* (23-24), pp.4559-4561.

[43] Huang, Y., Cheng, X., Li, Y., Yu, G., Xu, K. & Li, G., 2018. Effect of in-situ synthesized nano-mgo on thermal properties of nano3-kno3. *Solar Energy, 160*, pp.208-215.

[44] Alghool, S., El-Halim, A., Hanan, F. & Mostafa, A.M., 2019. An eco-friendly synthesis of v2o5 nanoparticles and their catalytic activity for the degradation of 4-nitrophrnol. *Journal of Inorganic and Organometallic Polymers and Materials, 29* (4), pp.1324-1330.